Assembly of the peripheral stalk of ATP synthase in human mitochondria

Jiuya He[1], Joe Carroll[1], Shujing Ding, Ian M. Fearnley, Martin G. Montgomery and John E. Walker[2]

Medical Research Council Mitochondrial Biology Unit, University of Cambridge, Cambridge Biomedical Campus, Hills Road, Cambridge CB2 0XY, United Kingdom

[1] Equal contributions

[2]To whom correspondence should be addressed. e-mail: walker@mrc-mbu.cam.ac.uk

Running title: Assembly of ATP synthase

The authors declare no conflict of interest

Author contributions: J. E. W. designed research and supervised project; J. H., J. C., S. D. and I. M. F. performed research; J. H., J. C., S. D., I. M. F. and J. E. W. analyzed data, J. H., J. C. and M. G. M. prepared the figures, and J. E. W. prepared the manuscript.

Classification: BIOLOGICAL SCIENCES, Biochemistry

Key words: human mitochondria; ATP synthase; assembly; peripheral stalk

Significance

The production of adenosine triphosphate (ATP) in mitochondria, requires the oxidation of energy rich compounds to generate a proton motive force (pmf), a chemical potential difference for protons, across the inner membrane. This pmf powers the ATP synthase, a molecular machine with a rotary action, to synthesize ATP. The assembly of human ATP synthase from twenty-seven nuclear encoded proteins and two mitochondrially encoded subunits in the inner organellar membrane involves the formation of intermediate modules representing the F_1-catalytic domain, the peripheral stalk and associated membrane subunits, and the c_8-ring in the membrane part of the rotor. Here, we describe how components of the peripheral stalk and three associated membrane subunits are assembled and introduced into the enzyme complex. (118 words)

Abstract

The ATP synthase in human mitochondria is a membrane bound assembly of 29 proteins of 18 kinds organized into F_1-catalytic, peripheral stalk (PS) and c_8-rotor ring modules. All but two membrane components are encoded in nuclear genes, synthesized on cytoplasmic ribosomes, imported into the mitochondrial matrix, and assembled into the complex with the mitochondrial gene products, ATP6 and ATP8. Intermediate vestigial ATPase complexes formed by disruption of nuclear genes for individual subunits provide a description of how the various domains are introduced into the enzyme. From this approach, it is evident that three alternative pathways operate to introduce the PS module (including associated membrane subunits e, f and g). In one pathway, the PS is built up by addition to the core subunit b of membrane subunits e and g together, followed by membrane subunit f. Then this b-e-g-f complex is bound to the preformed F_1-c_8 module by subunits OSCP and F_6. The final component of the PS, subunit d, is added subsequently to form a key intermediate that accepts the two mitochondrially encoded subunits. In another route to this key intermediate, first e and g together and then f are added

to a pre-formed F_1-c_8-OSCP-F_6-b-d complex. A third route involves the addition of the c_8-ring module to the complete F_1-PS complex. The key intermediate then accepts the two mitochondrially encoded subunits, stabilized by the addition of subunit j, leading to an ATP synthase complex that is coupled to the proton motive force and capable of making ATP. [248 words]

Introduction

Energy derived from oxidative metabolism generates a proton-motive force (pmf) across the inner membranes of mitochondria, which the ATP synthase harnesses to provide most cellular ATP from ADP and phosphate by a rotary catalytic mechanism (1–3). Human ATP synthase is closely related in subunit composition and sequences to the bovine enzyme (3). Bovine ATP synthase is a protein-lipid complex made from 29 protein subunits of 18 types, including a regulatory protein, IF_1 contributing a mass of 591 kDa, and five specifically bound phospholipids (Fig. 1 and *SI Appendix* Fig. S1) (3, 4). The protein subunits of the human enzyme are organized by an assembly process into membrane extrinsic and membrane intrinsic domains, linked by a central stalk and a peripheral stalk (PS) (5, 6). The PS is often taken to denote the membrane extrinsic region of the stator. Here, because of the way this region of the enzyme is assembled, the term PS signifies the membrane extrinsic region of the peripheral stalk plus the membrane intrinsic region of subunits b, and the associated supernumerary subunits e, f and g. Two additional subunits, known previously as 6.8PL (6.8 kDa proteolipid) and DAPIT (diabetes associated protein in insulin sensitive tissue) are referred to here according to the names of their yeast orthologs, subunits j and k, respectively (4, 5, 7–10). Fifteen of the seventeen kinds of subunits of human ATP synthase are nuclear gene products that are imported into the organelle, where they are assembled together to form the complete complex with the two remaining subunits ATP6 (or a) and ATP8 (or A6L), which are both encoded in mitochondrial DNA and synthesized in the mitochondrial matrix (11). Currently, it

is not known when the five phospholipids are incorporated into the complex (see Fig. S1). Previously, we have described the later stages of the assembly of nuclear encoded subunits of the membrane domain based upon editing specific human genes with CRISPR-Cas9, and by characterizing the partial vestigial ATP synthase complexes that assemble in these cells, and also by the study of the assembly process in ρ^0 cells, which lack mitochondrial DNA, and therefore are incapable of making subunits ATP6 and ATP8 (5, 12). From these studies an F_1-PS-c_8-ring complex has been identified as a fundamental assembly intermediate, that provides the template for insertion of the two mitochondrially encoded subunits ATP6 and ATP8 in an unknown order. Their insertion is completed by the addition of subunit j which augments the entry of ATP6, evidently by holding it in close juxtaposition to the c_8-ring as required for the formation of the trans-membrane proton pathway at the c_8-ring:ATP6 interface. On the basis of the structures of the monomer:monomer interface in the dimeric bovine and yeast ATP synthases (4, 13), the entry of subunit j also allows the monomeric complexes to associate into the dimeric complexes found along the edges of the cristae in mitochondria (14–17). The final subunit to be added, subunit k, may be involved, in tethering dimers into tetramers and higher oligomers (5, 18). Here, we describe routes for assembly and incorporation of the PS module into the complex.

Results

Human Cells Lacking Subunits d and F_6. *ATP5PD* and *ATP5PF* encoding, respectively, subunits d and F_6 of ATP synthase (*SI Appendix*, Fig. S2) were disrupted in HAP1-WT (wild-type) cells by CRISPR-Cas9 (*SI Appendix*, Tables S1 and S2, and Fig. S3). The resulting clonal cells, HAP1-Δd and HAP1-ΔF_6, lacked the edited subunits, and produced different vestigial complexes with PS subunits depleted or absent (Fig. 2, *SI Appendix*, Fig. S4). The removal of either subunit d or F_6 had little effect on the initial rate of cell proliferation, but after about 60-70 h, growth ceased and the confluence declined (*SI Appendix*, Fig. S5), probably because of

increased glycolysis and faster acidification of the culture medium in mutant cells than in WT cells under non-inhibited conditions (*SI Appendix*, Fig. S5). The deletion of subunit d or F_6 affected respiration severely (*SI Appendix*, Fig. S5), similar to the impact of individual removal of the OSCP or subunits b, c, e, f and g (5, 12, 19). The lack of effect of oligomycin on these cells indicated that any intermediate vestigial ATP synthases are uncoupled from pmf. The levels of complexes I, III, and IV, but not complex II, were lower in both mutant cells (*SI Appendix*, Fig. S6), with an associated lower respiratory capacity (*SI Appendix*, Fig. S5). The effect of removing the PS subunit F_6 had a greater impact on assembly (Fig. 2), and the vestigial complex in HAP1-ΔF_6 cells contained significant levels of only the five subunits from the F_1 domain and the membrane subunit c (Fig. 3*A*; *SI Appendix*, Fig. S7*A* and Datasets S1 and S2), consistent with the presence of a F_1-c_8 subcomplex, observed previously when either of two other PS constituent subunits, b or OSCP, was removed (19). The quantitative MS analysis (Fig. 3*A*) showed that the level of the vestigial F_1-c_8 complex in HAP1-ΔF_6 cells was reduced to *ca*. 50% of the level of intact ATP synthase in HAP1-WT cells. Similarly, in HAP1-Δd cells, the constituent subunits of the F_1-c_8 component were present at *ca*. 60-65% of the levels in WT cells, with the remaining PS and membrane subunits at *ca*. 30-40% of their WT abundances (Fig. 3*B*; *SI Appendix*, Fig. S7*B* and Datasets S3 and S4). Therefore, it appears that HAP1-Δd cells assemble both an F_1-c_8 subcomplex, and F_1-c_8 associated with a PS complex containing subunits OSCP, b, F_6, e, f and g. An alternative interpretation is that the F_1-c_8-OSCP-F_6-b-e-f-g vestigial complex in HAP1-Δd cells is somewhat unstable and dissociates partially during purification. The formation of the vestigial complexes in both derivative cells was accompanied by an elevation in the relative level of IF_1-M1, and a decrease in IF_1-M3 (Figs. 3*A* and 3*B*).

The quantitative relative levels of subunits in mitoplasts showed that removal of subunit d was accompanied by a substantial reduction in the levels of mitochondrially encoded ATP

synthase subunits ATP6 and ATP8, and the level of subunit j was reduced also (Figs. 3*D*, *SI Appendix*, Fig. S8*A* and Datasets S5 and S6). None of these three subunits is a component of the vestigial complex in HAP1-Δd cells. The low levels of ATP6, ATP8 and subunit j in mitoplasts may reflect a rapid turnover of unassembled subunits, or down-regulation of their expression in the absence of an assembled enzyme. A comparison of the relative levels of the other subunits in mitoplasts indicates a small excess of F_1-c_8 components, supporting the presence of both F_1-c_8 and F_1-c_8 associated with a PS complex containing subunits OSCP, b, F_6, e, f and g. The deletion of subunit F_6 was accompanied by a large decrease in the levels of subunits ATP6, ATP8 and d, and also low levels of b, OSCP, e, f, g and j, consistent with these cells forming predominantly a F_1-c_8 vestigial complex (Figs. 3*C*, *SI Appendix*, Fig. S8*B* and Datasets S7 and S8). In both mutant cells, the difference in the relative levels of subunit k in mitoplasts compared with the purified complexes was larger than for other ATP synthase subunits, indicating the presence of the free unassociated subunit.

Oligomeric State of Vestigial ATP Synthases. Analysis by both BN- and CN-PAGE of the vestigial ATP synthase from HAP1-ΔF_6 cells demonstrated the presence of a single dominant band, cross-reacting with an antibody for the α-subunit, at a position corresponding to a monomeric F_1-c_8 subcomplex of ATP synthase (s_1 in Fig. 4), supporting the quantitative analysis (Fig. 3*A*). A minor component at *ca.*160 kDa detected in CN-PAGE analysis contained at least the PS subunit b and supernumerary subunits e, f and g (s_2 in Fig. 4*B*), and a similar complex was detected in wild type cells. This b-e-g-f containing subcomplex was prominent in analyses by both BN- and CN-PAGE of samples from HAP1-Δd cells. These latter samples also contained the F_1-c_8 subcomplex (s_1), and additional bands detected in BN-PAGE gels could be monomeric (m) and dimeric (d) forms of a vestigial F_1-c_8-OSCP-F_6-b-e-f-g complex (Fig. 4*A*). As subunit j, the key dimerising component (4) is largely absent, the presence of dimers can be explained either by the face-to-back association of monomers via subunit g, or

by monomeric complexes linked, as in the structure of tetrameric porcine ATP synthase (20), by dimeric IF_1(21, 22). The IF_1-M1 form is consistently found at increased relative levels in the vestigial complexes (Fig. 3) (5, 12, 19). The quantitative mass spectrometric analyses suggested that HAP1-Δd cells produce both an F_1-c_8 and F_1-c_8-OSCP-F_6-b-e-f-g vestigial complex. The low intensity of the apparent monomeric and dimeric F_1-c_8-OSCP-F_6-b-e-f-g vestigial complexes, combined with the strong b-e-f-g band suggests that the F_1-c_8-OSCP-F_6-b-e-f-g vestigial complex may be unstable and give rise to the combination of complexes observed in the native gel analyses of samples from HAP1-Δd cells.

The b-e-g and b-e-g-f Subcomplexes of ATP Synthase. The formation of a b-e-g-f subcomplex in HAP1 cells was examined further in cell lines lacking individual subunits b, e, f, g and δ. It was demonstrated that the HAP1-Δe, -Δg and -Δf cells all form monomeric vestigial complexes containing the b-subunit, slightly smaller than intact monomeric ATP synthase, and that the complex formed by HAP1-Δf cells also contains subunits e and g (Fig. 5), as observed before by BN-PAGE (5). Also, HAP1-Δf cells produced a smaller b-e-g subcomplex of *ca.* 150 kDa and this subcomplex was not formed when any one of subunits b, e or g was deleted. A monomeric vestigial complex of *ca.*700 kDa was not observed in HAP1-Δδ cells, but they have a subcomplex of *ca.*160 kDa, containing subunits b, e, g and f, slightly larger than the b-e-g subcomplex as expected, and consistent with the assembly of a b-e-g-f subcomplex. The HAP1-Δδ cells also formed an uncharacterized 80 kDa complex containing subunit e.

Further evidence for the b-e-g-f complex was provided by the expression in HEK293-Δδ cells of the b-subunit with a C-terminal Flag-Strep II tag, and analysis of the purified complex of the tagged subunit and associated proteins by gel and mass spectrometric analyses. The HEK293-Δδ cell line was employed so as to favor the formation of the b-e-g-f subcomplex (*SI Appendix*, Fig. S9*A*), as in HAP1-Δδ cells (Fig. 5). The reciprocally labelled control sample

for this experiment was provided by HEK293-Δδ cells where a C-terminally tagged version of the subunit j (which is not part of the b-e-g-f complex) was expressed. There was no evidence for or against a specific complex containing subunit j in the HEK293-Δδ cells (Fig. 6), but, as the majority of the data points occupy the upper right quadrant, the choice of tagged subunit j as a control was sub-optimal. However, only subunits e, f and g were appreciably associated with the tagged b-subunit (Fig. 6), and therefore the experiment provides further evidence for the formation of the b-e-g-f intermediate.

Discussion

The bovine and human ATP synthases have the same subunit composition and the sequences of the subunits are highly conserved (3, 12, 23). Therefore, the structure of the bovine enzyme (Fig. 1) is an excellent surrogate for that of the human enzyme that can be employed in the interpretation of the pathway of assembly of the human complex. The structure illustrates that the protein components of the PS, the OSCP, b-, d-, F_6-, e-, f- and g-subunits, plus the ATP6- and ATP8-subunits, and the associated supernumerary membrane subunits j and k, constitute the enzyme's stator against which the rotor turns (4). The rotor consists of central stalk components, subunits γ, δ and ε, which is bound to a ring of eight c-subunits in the membrane domain (24). During catalysis, the PS prevents the dissociation of the $\alpha_3\beta_3$-domain from the central stalk by clamping it in position from above via interactions between the N-terminal regions of α-subunits with the N-terminal domain of the OSCP. Also, it resists the rotational torque of the central stalk, preventing the $\alpha_3\beta_3$-domain and the rest of the stator domain from following the direction of rotation. The structure of the PS is elongated and largely α-helical, and it illustrates the roles of its individual components. The N-terminal domain of the OSCP, attached to the F_1-domain, is linked to its C-terminal domain via a flexible region that provides a universal joint to accommodate the side-to-side rocking of the F_1-domain during catalysis. This C-terminal domain of the OSCP is bound to bH4, the C-terminal α-helix of subunit b. α-

Helix bH4 is attached to α-helix bH3, which extends about 150 Å through the core of the PS to the surface of the IMM and then across the membrane. Other α-helices in the F_6 and d-subunits, and another extending up from the membrane domain of subunit ATP8, are bound parallel to bH3, helping to rigidify most of the PS, except for a hinge in bH3 close to the membrane's surface that allows the PS to flex during catalysis. The membrane bound N-terminal region of the b-subunit is folded into two further α-helices, bH1and bH2, and together with the transmembrane domain of bH3, they form the skeleton of a wedge-shaped structure, with bH1 sitting on top on the matrix side of the IMM and transmembrane α-helices bH2 and bH3 subtending an angle of *ca.* 45° (*SI Appendix* Fig. S1). The association of the two wedges in the dimeric enzyme places the central rotatory axes of the monomeric enzymes at an angle to each other. The supernumerary subunits e, f and g also contribute to the structure of the wedge. The single transmembrane α-helices of each of subunits e and g augment α-helix bH2, and the top of the wedge on the matrix side of the membrane is provided by four amphipathic α-helices two in each of the g- and f-subunits, which lie in the lipid head-group region of the membrane. Internal cavities in the wedge are occupied by five specifically bound lipids, three cardiolipins (CDL1-CDL3) and two other lipids tentatively modelled as phosphatidyl glycerols (LHG4 and LHG5). These five lipids probably enhance the stability of the wedge (4).

In earlier studies of the assembly of the membrane domain of human ATP synthase, sub-complex (*D*) in Fig. 7 was characterized as a key intermediate in the later stages of the assembly process (5). It provides the template for the introduction of subunits ATP6 and ATP8, both encoded in mitochondrial-DNA, allowing the proton channel to be formed and then stabilized by the subsequent addition of subunit j, producing a coupled active ATP synthase. In subcomplex (*D*), the PS is already fully assembled. In the current work, other vestigial complexes have been characterized from the mitochondria of human cells, where various subunits of ATP synthase have been removed individually. They demonstrate that the PS is not

introduced into intermediate (*D*) by a unique route, but that there are at least three alternative paths for doing so (Fig. 7). In one path, illustrated in Fig. 7 (*A*) and (*B*), a b-e-g complex binds subunit f to form a b-e-g-f subcomplex. When the association of this assembly with F_1-c_8 was prevented for example in HAP1-ΔF_6 cells, then b-e-g-f did not accumulate (Fig. 4), presumably because it was degraded in the mitochondria. The b-e-g-f subcomplex is probably an authentic assembly intermediate as it forms in the absence of an assembled F_1-domain (Fig. 6), but it cannot be completely excluded that it is also the product of the breakdown of an F_1-c_8-PS sub-complex, for example, either metabolically or artefactually during extraction of the vestigial complex with detergent and subsequent gel analyses. For example, in HAP1-Δd cells (Fig. 4), the substantial amounts of b-e-g-f that were observed are likely to have arisen from partial dissociation of an unstable F_1-c_8-OSCP-F_6-b-e-f-g vestigial complex. A b-e-g complex, that probably contained subunit f also, has been described before in HeLa cells where subunit d had been depleted (25). According to Fig. 7, the b-e-g-f subcomplex then associates with the F_1-c_8 subcomplex in the presence of subunits OSCP and F_6, resulting in the formation of the substoichiometric intermediate (*C*). In a final step, the assembly of the PS is completed by the introduction of subunit d. In a second path to intermediate (*D*) in Fig. 7*E* and 7*F*, an F_1-c_8 subcomplex, already associated with a partial PS consisting of subunits OSCP, b, d and F_6, binds an e-g subcomplex, and then intermediate (*D*) is made by the addition of subunit f. In a third path, the intermediate (*D*) is formed by first the association of an F_1-domain with a fully assembled PS, and then completed by the addition of the c_8-ring. A fourth, but related pathway of assembly of human ATP synthase has been proposed based on the mass spectrometric analysis of protein complexes fractionated by native gel electrophoresis (26). Here, a b-e-g-f subcomplex becomes incorporated into a PS complex plus subunits ATP6, ATP8, j and k, which then associates with an F_1-c_8 sub-complex to produce the intact ATP synthase. From current knowledge, it is not possible to say which route, if any, is dominant, and under what

circumstances the alternative routes operate. In *S. cerevisiae*, subunit c, as well as ATP6 and ATP8, is encoded in the organellar genome. Here, an F_1-PS-ATP6-ATP8 subcomplex forms first and then the c_{10}-ring is incorporated (6). However, the formation of the intermediate subcomplex requires the participation of assembly factors Atp10, Atp23 and INAC (27). So far, no assembly factor has been found to be required for the assembly of the human PS (Fig. 6, *SI Appendix*, Fig. S7), although others are needed to assist in the assembly of the F_1-domain (28, 29), and creating the c_8-ring and/or its association with the F_1-domain (30).

The formation of a b-e-g complex followed by the addition of subunit f to make the b-e-g-f subcomplex is consistent with the structure of the wedge domain (4), since subunit f is bound partially to the external surface of subunit g (*SI Appendix*, Fig. S1). From consideration of the structure, it seems likely that phospholipids CDL2, LHG4, CDL3 and LHG5 will be added to the b-e-g complex (effectively a nascent wedge complex) at as yet unspecified points before the addition of subunit f, and that CDL1 will be added subsequently (*SI Appendix*, Fig. S1). The incorporation of these lipids into the wedge domain of the ATP synthase is part of the assembly process of the enzyme and it warrants further investigation. Another issue requiring clarification is at what stage of the assembly process do the monomeric complexes dimerize? Two types of dimer can form, made from either appropriate vestigial complexes or from the fully assembled monomeric complex. They are the classic front-to-back dimers held together by interactions between j-subunits (4) with the rotatory axes at a range of acute angles, and those arising by the association of two monomers (partially or fully assembled) across what will become the dimer-dimer interface in the rows of dimers observed in the cristae. The latter class could arise from interactions between k-subunits in each monomer (5), or they could be held together by dimeric IF_1 molecules bridging between the two catalytic F_1-domains (20, 21). Low levels of dimeric forms of vestigial ATP synthase complexes lacking subunit j have been observed in ρ^0, Δd and Δf cells (Fig. 4) (5, 12, 31), suggesting that they may be side-by-side

dimers. Conditions are known for extracting and purifying dimeric bovine complexes that have been verified by electron cryo-microscopy to be front-to-back dimers (4). Dimeric complexes are frequently observed in native gel analyses of extracts of mitochondrial membranes from wild-type and mutant cells, and are often assumed to be the classic type. However, the exact nature of the dimer cannot be ascertained with certainty without corroborative investigations, and improved protocols are required for the study of their involvement in the assembly of the ATP synthase.

Materials and Methods

Human genes *ATP5PD* and *ATP5PF* in HAP1 cells and *ATP5F1D* in HEK293 Flp-In™ T-REx™ cells were disrupted by CRISPR-Cas9 (32), leading to clonal cells HAP1-Δd, -ΔF_6, and HEK293-Δδ respectively. HAP1-WT and a clonal HAP1-Δδ cell were purchased from Horizon Discovery, Cambridge, U. K. The derivation of HAP1-Δb, -Δe, -Δf and Δg cells has been described before (5, 19). Plasmid pcDNA5™/FRT/TO encoding either subunit b or j, each with tandem C-terminal Strep II and FLAG tags was co-transfected with plasmid pOG44 in the presence of Lipofectamine 2000 (Invitrogen) into HEK293-Δδ cells, and stably transformed cells expressing the tagged subunits were selected. Cell proliferation was monitored with an Incucyte HD instrument (Essen Bioscience), and the oxygen consumption of cells was measured in a Seahorse XF^{e}24 analyzer (Agilent Technologies). The oligomeric state of ATP synthase and vestigial complexes was examined by BN- and CN-PAGE and Western blotting. ATP synthase and vestigial complexes were immuno-purified from mitoplasts, analyzed by SDS-PAGE with Coomassie blue staining, and by quantitative mass spectrometry of trypsin and chymotrypsin digests. For quantitative MS analyses, proteins were subject to stable isotope labelling in cell culture (SILAC). For details, see *SI Appendix*.

Acknowledgements. This work was supported by the MRC, U. K. via Programme grant MR/M009858/1 and grant MC_UU_00015/8 (to J. E. W.).

References

1. P. Mitchell, Coupling of phosphorylation to electron and hydrogen transfer by a chemi-osmotic type of mechanism. *Nature* **191**, 144-148 (1961).
2. J. E. Walker, The ATP synthase: the understood, the uncertain and the unknown. *Biochem. Soc. Trans.* **41**, 1-16 (2013).
3. J. E. Walker, "Chapter 13: Structure, mechanism and regulation of ATP synthases" in Mechanisms of primary energy transduction in biology, M. Wikström, Ed. (The Royal Society of Chemistry, 2017), pp. 338–373.
4. T. E. Spikes, M. G. Montgomery, J. E. Walker, Structure of the dimeric ATP synthase from bovine mitochondria. *Proc. Natl. Acad. Sci. U.S.A.* (2020), https://doi.org/10.1073/pnas.2013998117.
5. J. He*, et al.*, Assembly of the membrane domain of ATP synthase in human mitochondria. *Proc. Natl. Acad. Sci. U.S.A.* **115**, 2988-2993 (2018).
6. J. Song, N. Pfanner, T. Becker, Assembling the mitochondrial ATP synthase. *Proc. Natl. Acad. Sci. U.S.A.* **115**, 2850-2852 (2018).
7. I. Arnold, K. Pfeiffer, W. Neupert, R. A. Stuart, H. Schägger, Yeast mitochondrial F_1F_o-ATP synthase exists as a dimer: identification of three dimer-specific subunits. *EMBO J.* **17**, 7170-7178 (1998).
8. I. Arnold, K. Pfeiffer, W. Neupert, R. A. Stuart, H. Schägger, ATP synthase of yeast mitochondria. Isolation of subunit j and disruption of the ATP18 gene. *J. Biol. Chem.* **274**, 36-40 (1999).
9. R. Chen, M. J. Runswick, J. Carroll, I. M. Fearnley, J. E. Walker, Association of two proteolipids of unknown function with ATP synthase from bovine heart mitochondria. *FEBS Lett.* **581**, 3145-3148 (2007).

10. B. Meyer, I. Wittig, E. Trifilieff, M. Karas, H. Schägger, Identification of two proteins associated with mammalian ATP synthase. *Mol. Cell. Proteomics* **6**, 1690-1699 (2007).

11. I. M. Fearnley, J. E. Walker, Two overlapping genes in bovine mitochondrial DNA encode membrane components of ATP synthase. *EMBO J.* **5**, 2003-2008 (1986).

12. J. He*, et al.*, Persistence of the mitochondrial permeability transition in the absence of subunit c of human ATP synthase. *Proc. Natl. Acad. Sci. U.S.A.* **114**, 3409-3414 (2017).

13. H. Guo, S. A. Bueler, J. L. Rubinstein, Atomic model for the dimeric F_o region of mitochondrial ATP synthase. *Science* **358**, 936-940 (2017).

14. N. V. Dudkina, S. Sunderhaus, H. P. Braun, E. J. Boekema, Characterization of dimeric ATP synthase and cristae membrane ultrastructure from *Saccharomyces* and *Polytomella* mitochondria. *FEBS Lett.* **580**, 3427-3432 (2006).

15. M. Strauss, G. Hofhaus, R. R. Schröder, W. Kühlbrandt, Dimer ribbons of ATP synthase shape the inner mitochondrial membrane. *EMBO J.* **27**, 1154-1160 (2008).

16. N. V. Dudkina, G. T. Oostergetel, D. Lewejohann, H. P. Braun, E. J. Boekema, Row-like organization of ATP synthase in intact mitochondria determined by cryo-electron tomography. *Biochim. Biophys. Acta* **1797**, 272-277 (2010).

17. K. M. Davies*, et al.*, Macromolecular organization of ATP synthase and complex I in whole mitochondria. *Proc. Natl. Acad. Sci. U.S.A.* **108**, 14121-14126 (2011).

18. J. E. Walker, J. He, J. Carroll, "Chapter 6: Modular Assembly of ATP Synthase" in Oxygen Production and Reduction in Artificial and Natural Systems, J. Barber, A. V. Ruban, P. J. Nixon, Eds. (World Scientific Publishing, 2019), pp. 119–134.

19. J. He, J. Carroll, S. Ding, I. M. Fearnley, J. E. Walker, Permeability transition in human mitochondria persists in the absence of peripheral stalk subunits of ATP synthase. *Proc. Natl. Acad. Sci. U.S.A.* **114**, 9086-9091 (2017).

20. J. Gu, *et al.*, Cryo-EM structure of the mammalian ATP synthase tetramer bound with inhibitory protein IF1. *Science* **364**, 1068-1075 (2019).

21. E. Cabezón, I. Arechaga, P. J. G. Butler, J. E. Walker, Dimerization of bovine F_1-ATPase by binding the inhibitor protein, IF_1. *J. Biol. Chem.* **275**, 28353-28355 (2000).

22. E. Cabezón, M. J. Runswick, A. G. W. Leslie, J. E. Walker, The structure of bovine IF_1, the regulatory subunit of mitochondrial F-ATPase. *EMBO J.* **20**, 6990-6996 (2001).

23. T. B. Walpole, *et al.*, Conservation of complete trimethylation of lysine-43 in the rotor ring of c-subunits of metazoan adenosine triphosphate (ATP) synthases. *Mol. Cell. Proteomics* **14**, 828-840 (2015).

24. I. N. Watt, M. G. Montgomery, M. J. Runswick, A. G. W. Leslie, J. E. Walker, Bioenergetic cost of making an adenosine triphosphate molecule in animal mitochondria. *Proc. Natl. Acad. Sci. U.S.A.* **107**, 16823-16827 (2010).

25. M. Fujikawa, K. Sugawara, T. Tanabe, M. Yoshida, Assembly of human mitochondrial ATP synthase through two separate intermediates, F_1-c-ring and b-e-g complex. *FEBS Lett.* **589**, 2707-2712 (2015).

26. L. Sánchez-Caballero, *et al.*, TMEM70 functions in the assembly of complexes I and V. *Biochim. Biophys. Acta Bioenerg.* **1861**, 148202 (2020).

27. N. Naumenko, M. Morgenstern, R. Rucktäschel, B. Warscheid, P. Rehling, INA complex liaises the F_1F_o-ATP synthase membrane motor modules. *Nat. Commun.* **8**, 1237 (2017).

28. Z. G. Wang, P. S. White, S. H. Ackerman, Atp11p and Atp12p are assembly factors for the F_1-ATPase in human mitochondria. *J. Biol. Chem.* **276**, 30773-30778 (2001).

29. Y. Li, A. A. Jourdain, S. E. Calvo, J. S. Liu, V. K. Mootha, CLIC, a tool for expanding biological pathways based on co-expression across thousands of datasets. *PLoS Comput. Biol.* **13**, e1005653 (2017).

30. J. Kovalčíková, *et al.*, TMEM70 facilitates biogenesis of mammalian ATP synthase by promoting subunit c incorporation into the rotor structure of the enzyme. *FASEB J.* fj201900685RR (2019).

31. I. Wittig, *et al.*, Assembly and oligomerization of human ATP synthase lacking mitochondrial subunits a and A6L. *Biochim. Biophys. Acta* **1797**, 1004-1011 (2010).

32. F. A. Ran, *et al.*, Genome engineering using the CRISPR-Cas9 system. *Nat. Protoc.* **8**, 2281-2308 (2013).

33. L. A. Baker, I. N. Watt, M. J. Runswick, J. E. Walker, J. L. Rubinstein, Arrangement of subunits in intact mammalian mitochondrial ATP synthase determined by cryo-EM. *Proc. Natl. Acad. Sci. U.S.A.* **109**, 11675-11680 (2012).

34. C. Jiko, *et al.*, Bovine F_1F_o ATP synthase monomers bend the lipid bilayer in 2D membrane crystals. *Elife* **4**, e06119 (2015).

35. T. B. Blum, A. Hahn, T. Meier, K. M. Davies, W. Kühlbrandt, Dimers of mitochondrial ATP synthase induce membrane curvature and self-assemble into rows. *Proc. Natl. Acad. Sci. U.S.A.* (2019).

FIGURES

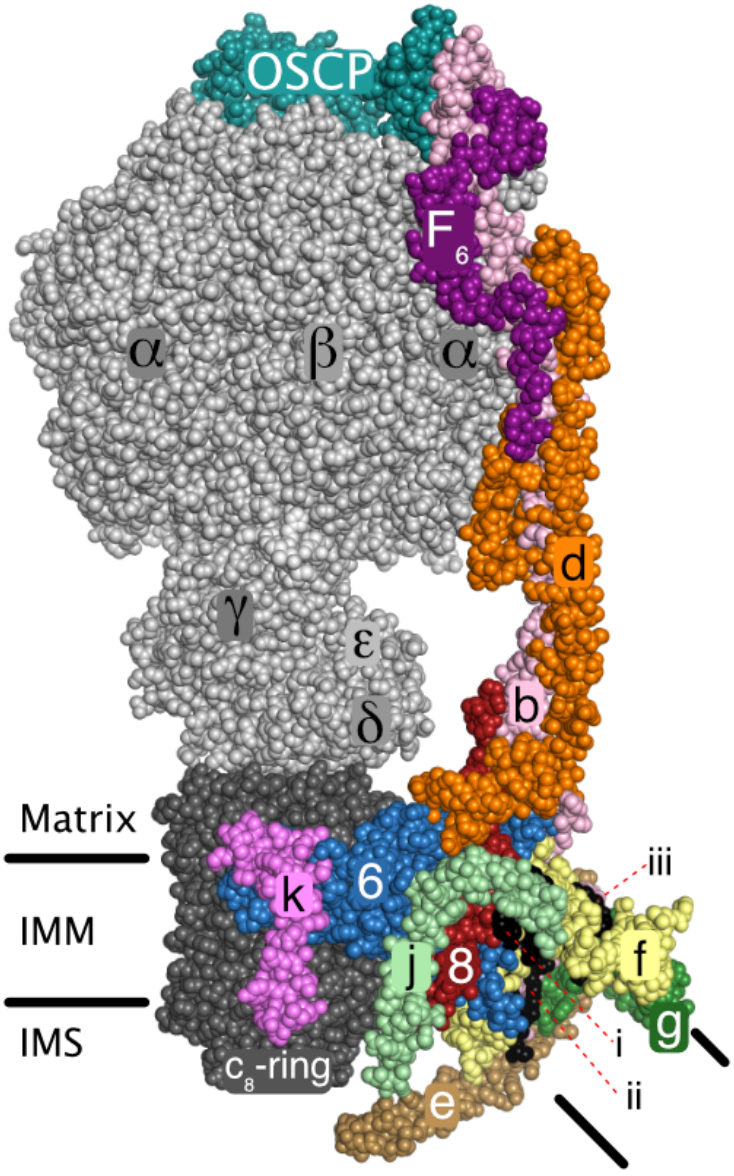

Fig. 1. Organization of peripheral stalk and associated subunits in a monomer in dimeric ATP synthase in bovine mitochondria. The enzyme is inhibited by residues 1-60 of the inhibitor protein IF_1, which is bound to the catalytic domain and not defined in the Figure (4). Black horizontal lines represent the inner mitochondrial membrane (IMM) separating the matrix from the intermembrane space (IMS). The PS is formed from subunits OSCP, F_6, d,

ATP8 (designated “8”) and b. Subunit b has two transmembrane α-helices, residues 33-47 of bH2 and residues 55-73 of bH3, with an angle of 45° between them. The N-terminal amphipathic α-helix, bH1 (residues 19-29), lies in the lipid head group region on the matrix side of the membrane. These three α-helices form the scaffold for a wedge structure in the membrane domain to which subunits e, f, g, j and ATP8, all with single transmembrane α-helices, are associated. Voids between proteins in the wedge are filled with five specifically bound lipids, three cardiolipins and two other lipids, tentatively modelled as phosphatidylglycerols (4). The positions of one cardiolipin (defined as CDL1), and the two phosphatidyl glycerols (defined as LHG4 and LHG5) are indicated by i-iii, respectively. The wedge braces ATP6 against the c_8-ring and in the dimer the two interacting wedges hold the rotatory axes of the monomeric enzymes at a range of acute angles via pivoting about the j-subunits in the surfaces of the two wedges (4). Subunit j is involved in the monomer-monomer interface in yeast mitochondria (13), but the interactions are different than in the bovine structure (4). Subunits e and g make a separate domain not in contact with ATP6 (designated “6”) and subunit j, that may promote inner membrane curvature (33–35). Subunit k may be involved in tethering dimers together (5). The mitochondrial pmf drives the rotation of the c_8-ring and the attached central stalk (subunits γ, δ and e) by the translocation of protons through the interface between the c_8 ring and ATP6. The rotation of the central stalk carries energy into the catalytic sites of the three β-subunits in the F_1-domain (subunit composition $\alpha_3\beta_3\gamma\delta e$).

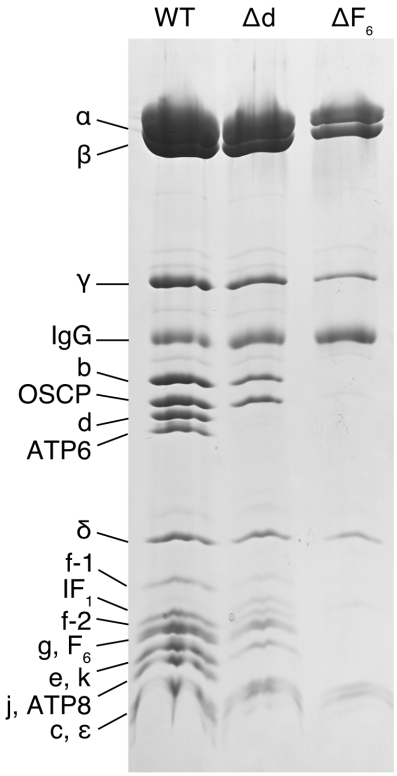

Fig. 2. Vestigial ATP synthase complexes in HAP1 cells devoid of peripheral stalk subunits d and F_6. Subunit compositions of vestigial human ATP synthase complexes in HAP1-Δd and HAP1-ΔF_6 cells. The vestigial complexes were immuno-purified from digitonin extracts of mitoplasts, fractioned by SDS-PAGE, and proteins were detected with Coomassie blue dye. The positions of subunits are indicated on the left.

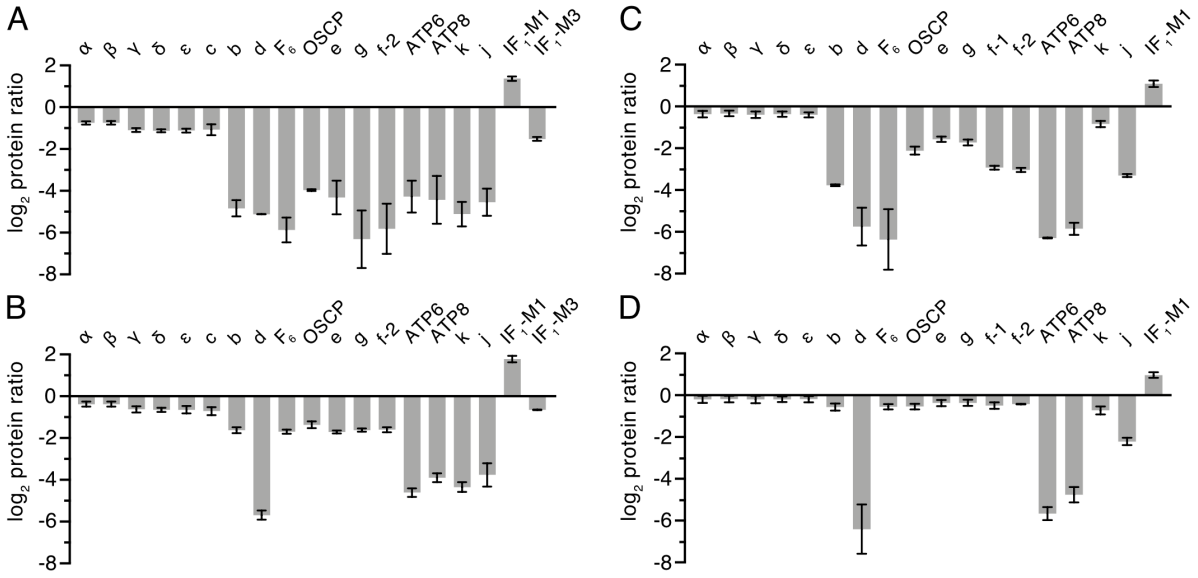

Fig. 3. Impact of removal of either subunit F_6 or d on the composition of vestigial ATP synthase complexes. Relative abundances of subunits and the inhibitor protein IF_1 in HAP1-ΔF_6 or HAP1-Δd cells, respectively, (*A* and *B*) in immunopurified vestigial complexes of ATP synthase, or (*C* and *D*) in digitonin solubilized mitoplasts. IF_1-M1 and -M3 are specific mature forms of IF_1(5), and f-1 and f-2 are isoforms of subunit f (Swiss-Prot P56134). The digitonin extracts of mitoplasts were prepared from 1:1 mixtures of differentially SILAC-labeled HAP1-WT cells plus either HAP1-ΔF_6 or HAP1-Δd cells, and complexes were purified from these samples. The purified samples were digested separately, in-solution, with trypsin or chymotrypsin, and mitoplast samples were separated by SDS-PAGE and digested in-gel with trypsin. Peptide mixtures were fractionated by reverse phase HPLC and analyzed by mass spectrometry. The histograms are the median values of both relative abundance ratios determined for proteins found in the complementary SILAC experiments. The protein ratio is derived from a minimum of two peptide ratios from each experiment, except for ATP6 (*B* and *D*), control heavy isotope experiments), f-2 (*D*, both experiments), and IF_1-M1 (*D*, control light isotope experiment), where all values are from a single peptide ratio. In mitoplast samples, no ratios were obtained for subunit-c or IF_1-M3 (*C* and *D*). The data for the identified proteins are given in *SI Appendix*, Datasets S1-S8. Error bars show the range of the two values.

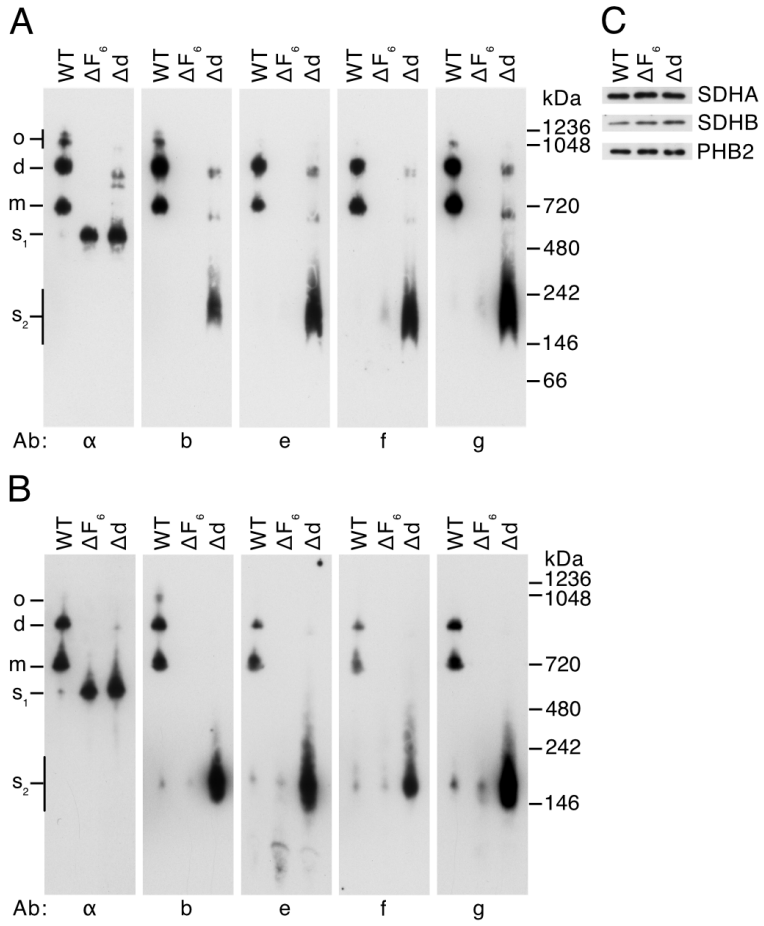

Fig. 4. Oligomeric states of ATP synthase and vestigial complexes in HAP1 cells. Mitochondrial membranes from HAP1-WT, -ΔF_6 and -Δd cells were extracted with digitonin (6 g/g protein). (*A* and *B*), Fractionation of extracts by BN-PAGE and CN-PAGE, respectively. Complexes were revealed by Western blotting with antibodies against various subunits of ATP synthase (indicated below the panels). The positions of complexes are shown on the left: o, oligomers; d, dimers; m, monomers; s_1, F_1-c_8 subcomplex; s_2, subcomplexes containing subunits b, e, f and g. The positions of molecular weight markers are shown on the right. (*C*), assessment of sample loading by Western blotting of digitonin extracts, fractionated by SDS-PAGE, with antibodies against the SDHA and SDHB subunits of complex II and prohibitin 2 (PHB2).

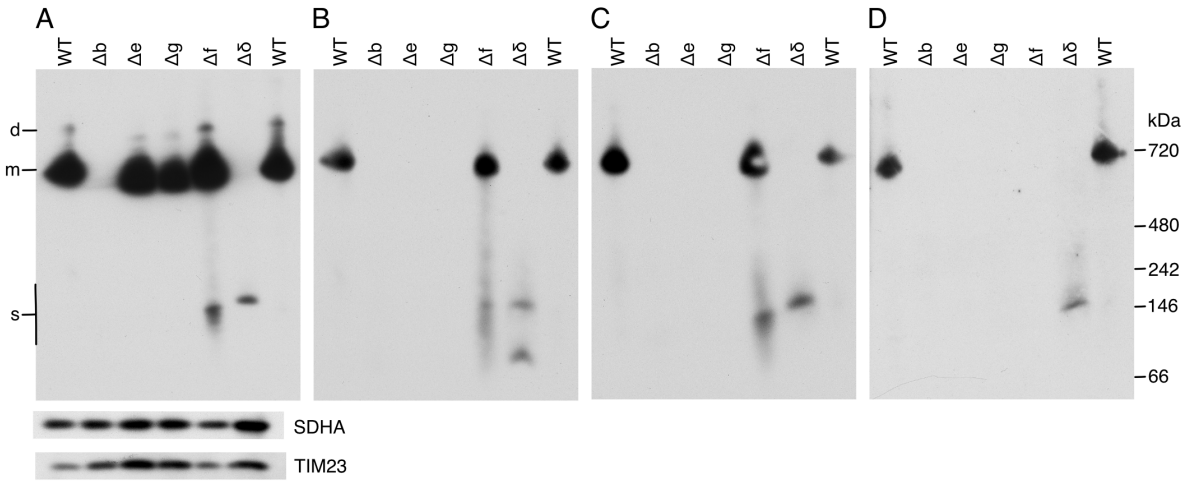

Fig. 5. Oligomeric states of ATP synthase and vestigial forms in HAP1-WT, -Δb, -Δe, -Δg, -Δf and -Δδ cells. ATP synthase and vestigial complexes were extracted from mitoplasts with digitonin (12 g/g protein). Extracts were fractioned by CN-PAGE and complexes detected with antibodies against individual subunits of ATP synthase. (*A*), subunit b. (*B*), subunit e. The lower band in the Δδ lane is probably free subunit e. (*C*), subunit g. (*D*), subunit f. The SDHA subunit of complex II and TIM23 are loading controls. On the left, d, and m, dimeric and monomeric ATP synthase, respectively; s, subcomplex b-e-g-f in Δδ samples, and b-e-g in HAP1-Δf samples. The positions of protein markers are shown on the right.

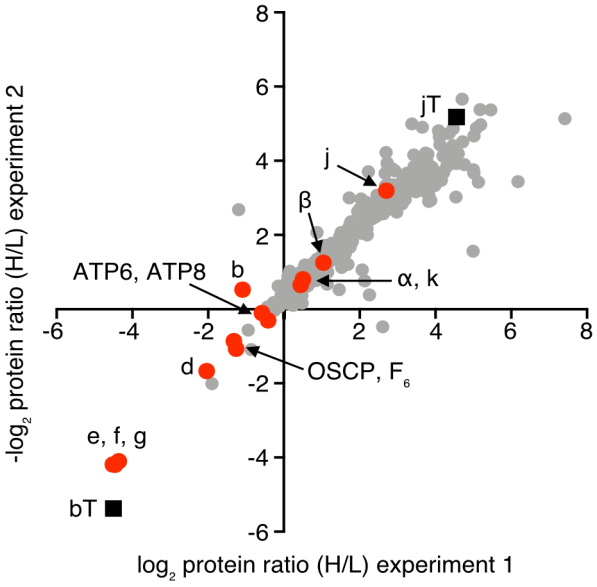

Fig. 6. Proteins associated with subunits b and j in HEK293T-Δδ cells. Quantitative mass spectrometry of affinity purified Flag-Strep II tagged subunit b (bT) and subunit j (jT), and

associated proteins. SILAC-labeled HEK293T-Δδ Flp-In™ T-REx™ cells individually overexpressing the tagged proteins were grown separately, combined and mitoplast samples prepared by a mild digitonin treatment. Proteins in mitoplast samples were extracted using digitonin at a higher detergent:protein ratio of 12:1 (g/g), and tagged plus associated proteins were purified by Strep II affinity chromatography. The experiment was performed twice, with reciprocal SILAC labeling orientations. ■, tagged proteins. ●, ATP synthase subunits. ●, Other proteins. Each data point corresponds to the abundance ratio of an identified protein from the two complementary experiments. The data for all of the identified proteins are given in *SI Appendix*, Datasets S9-S11.

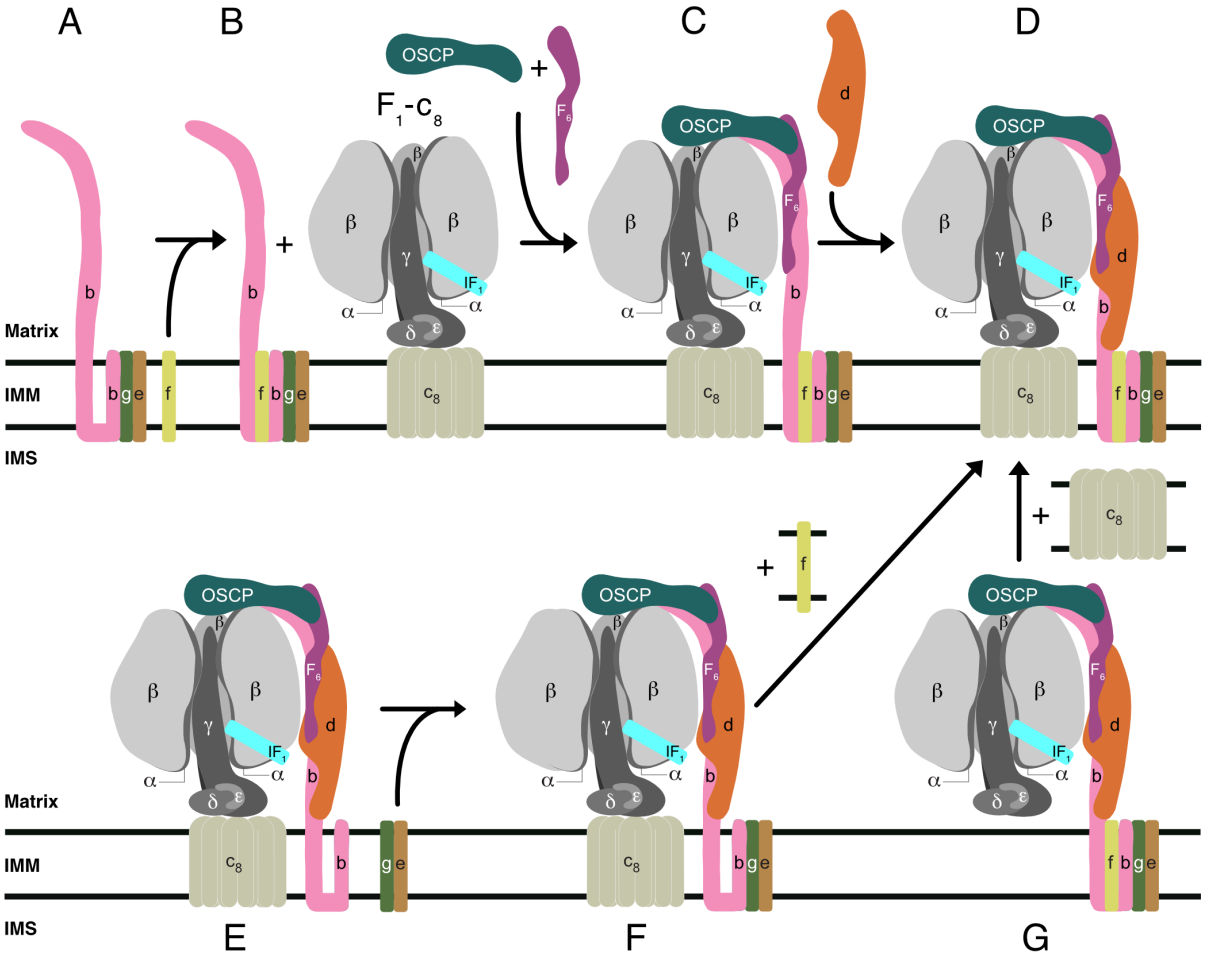

Fig. 7. Pathway(s) of assembly of the PS of human ATP synthase. (*A* and *B*) a tertiary b-e-g complex observed in HAP1-Δf cells binds subunit f to form the complex observed in HAP1-

Δδ cells; (*C*) in the presence of the OSCP and F_6, the b-e-g-f subcomplex binds to the F_1-c_8, complex to form the partially stable F_1-c_8-OSCP-F_6-b-e-g-f subcomplex observed in HAP1-Δd cells. (*D*) the stable key intermediate vestigial complex observed in ρ^0 cells is formed by the addition of the d-subunit; (*E* and *F*), two additional pathways of arriving at intermediate (*D*); in (*E*), a partly stable vestigial complex observed in HAP1-Δe and -Δg cells is elaborated by the addition of subunits e and g to form complex (*F*) observed in HAP1-Δf cells; alternatively in (*G*) key intermediate (*D*) is formed from (*G*) observed in HAP1-Δc cells of the independently assembled c_8-ring. Black horizontal lines represent the inner mitochondrial membrane (IMM) separating the matrix from the intermembrane space (IMS).

SI Appendix for:

Assembly of the peripheral stalk of ATP synthase in human mitochondria

Jiuya He[1], Joe Carroll[1], Shujing Ding, Ian M. Fearnley, Martin G. Montgomery and John E. Walker[2]

Medical Research Council Mitochondrial Biology Unit, University of Cambridge, Cambridge Biomedical Campus, Hills Road, Cambridge CB2 0XY, United Kingdom

Materials and Methods

Gene Disruptions. *ATP5PD* and *ATP5PF* encoding the d and F_6 subunits were disrupted individually in human HAP1-WT cells by CRISPR-Cas9 technology (1). Their structures are shown in *SI Appendix*, Fig. S2. HAP1 cells have a haploid karyotype, except for the presence of a fragment of chromosome 15 in chromosome 19 and a reciprocal translocation between chromosomes 9 and 22 (2, 3). None of these features affects the genes in question, as *ATP5PD* and *ATP5PF* are on chromosomes 17 and 21, respectively. For *ATP5PD* a pair of gRNAs characteristic of exon II and intron B were selected, and for *ATP5PF* the gRNA pair were both targeted to exon II (*SI Appendix*, Table S1). Each pair was introduced independently into HAP1-WT cells, and screening of clones from single cells for the absence of subunit d or F_6 led to the identification of HAP1-Δd, and -ΔF_6 cells. The changes introduced into *ATP5PD* and *ATP5PF* were sequenced with specific primers (*SI Appendix*, Table S2), showing that deletions had been introduced of 121 and 93 bp, respectively (*SI Appendix*, Fig. S3). Each deletion had arisen from two gRNAs and was mediated by non-homologous end-joining of the deleted genomic DNA. The deletion in *ATP5PD* left only the translational start codon in exon II, and also removed two bases of intron B, resulting in the termination of translation after 6 amino acids. An in-frame deletion in exon II of *ATP5PF* removed codons for amino acids 13-43,

encompassing 20 residues of the mitochondrial targeting sequence and 11 amino acids at the N-terminus of the mature protein sequence. There was no evidence of the targeted protein in mitoplast samples from these cells (*SI Appendix*, Fig. S4). The HAP1-Δδ cells were purchased from Horizon Discovery (Cambridge, U. K.) who had used the single gRNA GCTGGTCGTGGTGCATGCA to disrupt the gene. The targeted region of the *ATP5F1D* gene was amplified by PCR with the forward and reverse primers 5'-GTGCCTCACATCAGCGCCAGGTC-3' and 5'-AGCAGGGTCCCCTCTGGTTCGC-3', respectively. This G-C rich region was sequenced by dGTP chemistry (Source Bioscience) showing that the mutation had been introduced into the same location as described previously in a HAP1-Δ(c+δ) cell line (4). The production and characterization of HAP1-Δb, -Δe, -Δf, and -Δg cells have been described previously (5, 6).

Human *ATP5F1D*, encoding the δ-subunit of ATP synthase was disrupted in a HEK293 Flp-In™ T-REx™ cell by CRISPR-Cas9 with the same gRNA used for HAP1 cells. The targeted region was amplified by PCR with the same primers that were used in HAP1 cells. The two resulting fragments observed by agarose gel electrophoresis were gel purified (QIAquick gel extraction kit, Qiagen), cloned into the pCR4-TOPO vector (Thermo Scientific), and sequenced with M13 forward and reverse primers, and the dGTP chemistry method (Source Bioscience). The HEK293-Δδ clonal cell is unable to produce a functional δ-subunit (Fig. S9 and S10). An aberrant 17-18 kDa protein of unknown sequence observed in SDS lysates of cells and mitoplasts of HEK293-Δδ cells cross-reacted with an anti-δ antibody, but it was unable to promote assembly of intact ATP synthase, as shown by native gel analysis (Fig. S9).

Cell Culture. HAP1-WT (Horizon Discovery) and clonal cells were cultured in Iscove's modified Dulbecco's medium under standard conditions (7). Cell proliferation was monitored with an Incucyte HD instrument (Essen Bioscience) and oxygen consumption rate (OCR) was

measured in a Seahorse XF^{e}24 analyzer (Agilent Technologies), as described before (7). OCR was normalized to cell number by the sulforhodamine B assay (8). Stable isotope labelling of proteins with amino acids in cell culture (SILAC) (9) of HAP1-WT and gene disrupted clonal cells was carried out as described before (7).

Expression and Affinity Purification of Tagged ATP Synthase Subunits. Plasmid pcDNA5^{TM}/FRT/TO encoding subunit b or j, with tandem C-terminal Strep II and FLAG tags (10) was co-transfected in the presence of Lipofectamine 2000 (Invitrogen) with plasmid pOG44 into human HEK293-Δδ Flp-In^{TM}T-REx^{TM} cells (total DNA, 1 μg; pOG44:pcDNA5/FRT/TO, 7:1 by weight). After 24 h, the medium was replaced with the selective medium containing blasticidin (10 μg/ml) and hygromycin (100 μg/ml) and inducible cell clones expressing the recombinant protein were picked and verified by Western blotting of cell lysates with an anti-Strep II antibody. SILAC-labelling of cell proteins in culture was performed as described before (11), and expression of tagged subunits was induced for 72 h with doxycycline (20 ng/ml) prior to harvesting the cells. The SILAC DMEM media was also supplemented with 20 mM HEPES (pH 7.4) to aid buffering of the increased acidification of the media by these cell clones. Reciprocally labelled HEK293T-Δδ-bT (tagged subunit-b) and HEK293T-Δδ-jT (tagged j subunit) were mixed 1:1 (protein w/w). Mitoplast material was prepared by digitonin treatment (11, 12) and then solubilized with digitonin (12 g/g protein) for affinity purification of tagged subunits and associated proteins. A sample was loaded at 4ºC onto a Pierce spin column (0.9 ml; Thermo Fisher Scientific) containing Strep-Tactin-Sepharose (IBA Lifesciences) and then washed with 5 column volumes of buffer [20 mM HEPES, pH 7.6, 150 mM NaCl, 2 mM dithiothreitol, 1x cOmplete EDTA-free protease inhibitor (Roche), and 0.05% (w/v) digitonin]. Bound protein was eluted with 6 portions of 0.5 column volumes of buffer containing 10 mM desthiobiotin. Eluates were analyzed by SDS-PAGE and quantitative mass spectrometry. A distinction was made between the endogenous

subunits and the tagged form by the different migration positions on the SDS-PAGE gel. From the MaxQuant evidence file for the appropriate gel sections, the protein ratios of the tagged and endogenous subunits were determined manually (*SI appendix*, Datasets S10 and S11).

General Methods. Cell protein concentrations were determined by either the bicinchoninic acid assay (Thermo Fisher Scientific) or the detergent compatible protein assay (BioRad). Mitoplasts were prepared from cells with digitonin, as described before (11, 12). Extracts of mitoplasts made with dodecylmaltoside (DDM; 1%, w/v) were fractionated by SDS-PAGE, and subunits of ATP synthase and citrate synthase were detected by Western blotting. The oligomeric states of ATP synthase and vestigial complexes in digitonin extracts of mitoplasts were examined by BN-PAGE or CN-PAGE (13, 14), and Western blotting. Samples of mitoplasts were re-suspended to *ca.* 5 mg/ml in NativePAGE sample buffer (Thermo Fisher Scientific) containing digitonin (6-12 g/g protein), kept at 4°C for 15 min, and then centrifuged (10,500 x *g*, 20 min, 4°C). The supernatants were treated with benzonase (Merck Millipore) at room temperature, centrifuged again, and soluble complexes fractionated at 4°C in 3-12% acrylamide gradient Bis-Tris gels (Thermo Fisher Scientific) by CN-PAGE, or BN-PAGE according to the manufacturer's instructions for Western blotting. For CN-PAGE the cathode running buffer contained 0.05% (w/v) sodium deoxycholate plus 0.005% (w/v) DDM. The gel resolved complexes were transferred to polyvinylidene fluoride membranes, and the membranes were probed with subunit specific antibodies. The origins of the antibodies either have been described before (5, 6), or they are listed in *SI Appendix* Table S3. ATP synthase was purified from digitonin solubilized mitoplasts with an immuno-capture resin (Abcam) as described before (7). Proteins in SILAC labelled mitoplast samples for quantitative mass spectrometric analysis were reduced and alkylated in gel sample buffer, fractionated by SDS-PAGE and stained with Coomassie blue R250 dye (15). Stained gel sections were excised and proteins digested in-gel with trypsin (16). SILAC labelled and affinity purified samples of ATP

synthase were ethanol precipitated at -20ºC for 18 h with 20 vol. cold ethanol, centrifuged, and the pellet was digested in 50 mM ammonium bicarbonate for 18 h, with either trypsin at 37ºC or chymotrypsin at 30ºC.

Protein Quantitation. Relative quantitation of proteins was derived from mass spectrometric data of SILAC samples (9). Peptide mixtures was analyzed by LC-MS-MS on a Proxeon EASY-nLC1000 system coupled directly to a Q-Exactive+ Orbitrap mass spectrometer (Thermo Fisher Scientific). Heavy and light peptide mass data were analyzed with MaxQuant version 1.6.5.0, and the integrated Andromeda search engine (17, 18) employing a Swiss-Prot human protein database (March 2019) modified to include mature forms of ATP5IF1, denoted as IF_1-M1, -M2 and -M3, with N-terminal residues Phe-25, Gly-26 and Ser-27, respectively (19, 20), and a mature ATP synthase c-subunit. The ATP synthase c-subunit is encoded by three genes (21, 22), with different mitochondrial targeting pre-sequences, but identical mature protein sequences. To aid identification of this subunit, using peptides derived from the mature protein N-terminal sequence, a representative sequence (lacking the mitochondrial N-terminal import sequence) was added to the human protein database employed in these analyses, with the identifier P48201-M. In addition, lysine trimethylation was included when interrogating chymotrypsin digest data, to aid identification of a characteristic methylated subunit-c peptide (23). Search parameters for in-gel trypsin digest samples were: MS tolerance 4.5 p.p.m.; MS/MS tolerance 20 p.p.m.; Trypsin/P with two missed cleavages; Fixed modification - Cys-carbamidomethyl; variable modifications - oxidation (Met) and acetyl (protein N-terminus); Arg-10 and Lys-8. In solution digest sample parameters were: MS tolerance 4.5 p.p.m.; MS/MS tolerance 20 p.p.m.; trypsin/P with two missed cleavages; chymotrypsin with four missed cleavages; variable modifications - oxidation (Met), acetyl (protein N-term) and trimethyl (lysine); Arg-10 and Lys-8. The MaxQuant output was managed further with Perseus (24). Protein ratios for ATP5IF1 were calculated manually with data for the unique N-terminal

peptides of the various mature forms of ATP5IF1, located in the MaxQuant evidence file, and represent the median of the assigned specific peptide ratios, where MaxQuant ISO-MSMS peptide values were used only if fewer than three MULTI-MSMS peptide ratios were obtained. The basis of quantitative experiments using SILAC has been described previously (25).

References

1. F. A. Ran*, et al.*, Genome engineering using the CRISPR-Cas9 system. *Nat. Protoc.* **8**, 2281-2308 (2013).
2. J. E. Carette*, et al.*, Ebola virus entry requires the cholesterol transporter Niemann-Pick C1. *Nature* **477**, 340-343 (2011).
3. P. Essletzbichler*, et al.*, Megabase-scale deletion using CRISPR/Cas9 to generate a fully haploid human cell line. *Genome Res.* **24**, 2059-2065 (2014).
4. J. Carroll, J. He, S. Ding, I. M. Fearnley, J. E. Walker, Persistence of the permeability transition pore in human mitochondria devoid of an assembled ATP synthase. *Proc. Natl. Acad. Sci. U.S.A.* **116**, 12816-12821 (2019).
5. J. He, J. Carroll, S. Ding, I. M. Fearnley, J. E. Walker, Permeability transition in human mitochondria persists in the absence of peripheral stalk subunits of ATP synthase. *Proc. Natl. Acad. Sci. U.S.A.* **114**, 9086-9091 (2017).
6. J. He*, et al.*, Assembly of the membrane domain of ATP synthase in human mitochondria. *Proc. Natl. Acad. Sci. U.S.A.* **115**, 2988-2993 (2018).
7. J. He*, et al.*, Persistence of the mitochondrial permeability transition in the absence of subunit c of human ATP synthase. *Proc. Natl. Acad. Sci. U.S.A.* **114**, 3409-3414 (2017).
8. P. Skehan*, et al.*, New colorimetric cytotoxicity assay for anticancer-drug screening. *J. Natl. Cancer Inst.* **82**, 1107-1112 (1990).

9. S. E. Ong, *et al.*, Stable isotope labeling by amino acids in cell culture, SILAC, as a simple and accurate approach to expression proteomics. *Mol. Cell. Proteomics* **1**, 376-386 (2002).

10. J. He, *et al.*, Human C4orf14 interacts with the mitochondrial nucleoid and is involved in the biogenesis of the small mitochondrial ribosomal subunit. *Nucleic Acids Res.* **40**, 6097-6108 (2012).

11. V. F. Rhein, *et al.*, Human METTL20 methylates lysine residues adjacent to the recognition loop of the electron transfer flavoprotein in mitochondria. *J. Biol. Chem.* **289**, 24640-24651 (2014).

12. P. Klement, L. G. Nijtmans, C. Van den Bogert, J. Houstěk, Analysis of oxidative phosphorylation complexes in cultured human fibroblasts and amniocytes by blue-native-electrophoresis using mitoplasts isolated with the help of digitonin. *Anal. Biochem.* **231**, 218-224 (1995).

13. H. Schägger, G. von Jagow, Blue native electrophoresis for isolation of membrane protein complexes in enzymatically active form. *Anal. Biochem.* **199**, 223-231 (1991).

14. I. Wittig, M. Karas, H. Schägger, High resolution clear native electrophoresis for in-gel functional assays and fluorescence studies of membrane protein complexes. *Mol. Cell. Proteomics* **6**, 1215-1225 (2007).

15. V. F. Rhein, J. Carroll, S. Ding, I. M. Fearnley, J. E. Walker, NDUFAF7 methylates arginine 85 in the NDUFS2 subunit of human complex I. *J. Biol. Chem.* **288**, 33016-33026 (2013).

16. M. Wilm, *et al.*, Femtomole sequencing of proteins from polyacrylamide gels by nano-electrospray mass spectrometry. *Nature* **379**, 466-469 (1996).

17. J. Cox, M. Mann, MaxQuant enables high peptide identification rates, individualized p.p.b.-range mass accuracies and proteome-wide protein quantification. *Nat. Biotechnol.* **26**, 1367-1372 (2008).

18. J. Cox*, et al.*, Andromeda: a peptide search engine integrated into the MaxQuant environment. *J. Proteome Res.* **10**, 1794-1805 (2011).

19. G. Xu, S. B. Shin, S. R. Jaffrey, Global profiling of protease cleavage sites by chemoselective labeling of protein N-termini. *Proc. Natl. Acad. Sci. U.S.A.* **106**, 19310-19315 (2009).

20. A. S. Vaca Jacome*, et al.*, N-terminome analysis of the human mitochondrial proteome. *Proteomics* **15**, 2519-2524 (2015).

21. M. R. Dyer, J. E. Walker, Sequences of members of the human gene family for the c subunit of mitochondrial ATP synthase. *Biochem. J.* **293**, 51-64 (1993).

22. W. L. Yan, T. J. Lerner, J. L. Haines, J. F. Gusella, Sequence analysis and mapping of a novel human mitochondrial ATP synthase subunit 9 cDNA (ATP5G3). *Genomics* **24**, 375-377 (1994).

23. T. B. Walpole*, et al.*, Conservation of complete trimethylation of lysine-43 in the rotor ring of c-subunits of metazoan adenosine triphosphate (ATP) synthases. *Mol. Cell. Proteomics* **14**, 828-840 (2015).

24. S. Tyanova*, et al.*, The Perseus computational platform for comprehensive analysis of (prote)omics data. *Nat. Methods* **13**, 731-740 (2016).

25. J. Cox, M. Mann, Quantitative, high-resolution proteomics for data-driven systems biology. *Annu. Rev. Biochem.* **80**, 273-299 (2011).

26. T. E. Spikes, M. G. Montgomery, J. E. Walker, Structure of the dimeric ATP synthase from bovine mitochondria. *Proc. Natl. Acad. Sci. U.S.A.* In Press (2020).

Results

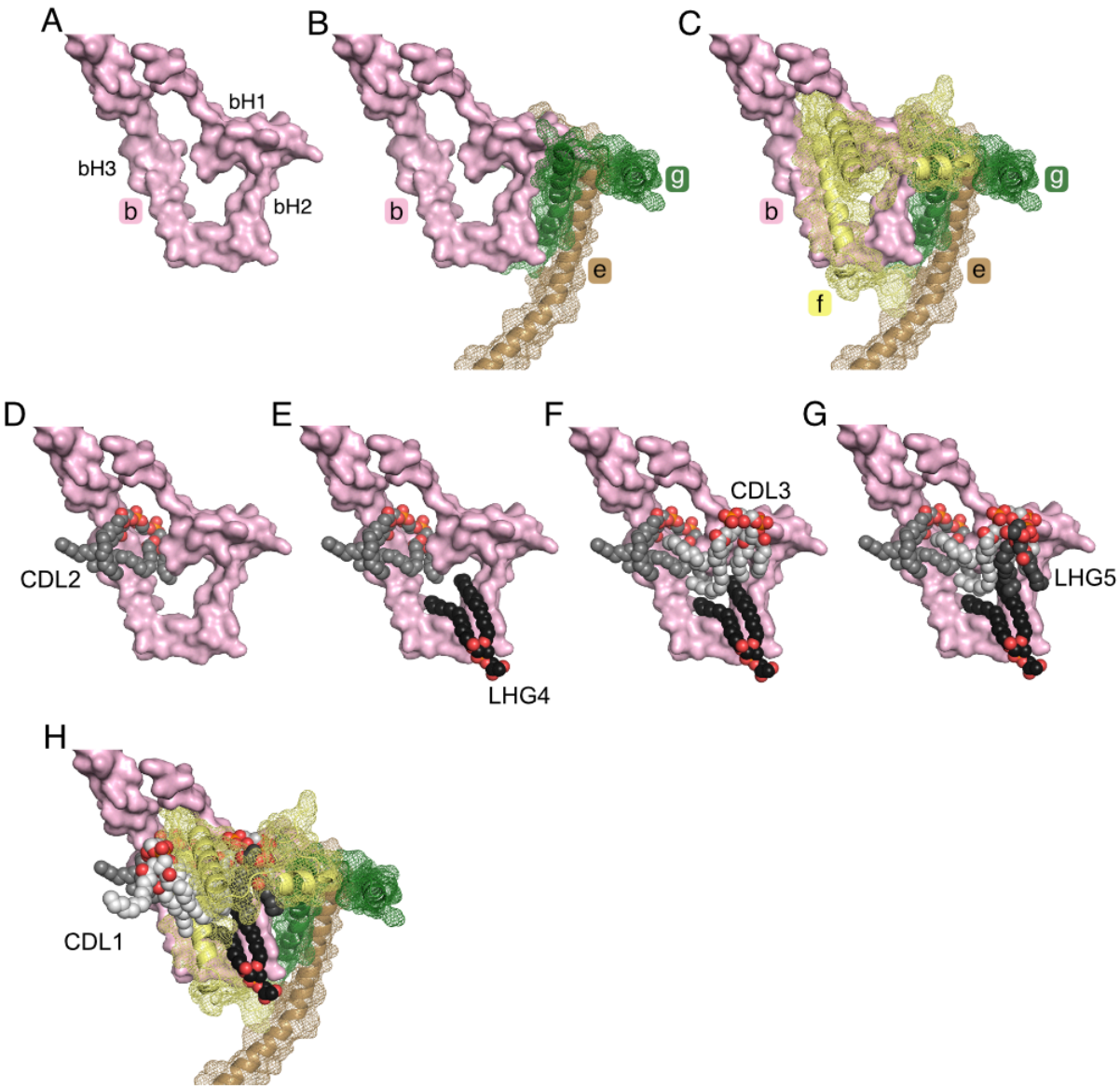

Fig. S1. Structure of wedge components in the membrane domain of bovine ATP synthase and possible points and order of incorporation of lipids into the wedge in the human enzyme. See (26). *A*, the membrane domain of subunit b, viewed orthogonal to the plane of the IMM, consisting of amphipathic α-helix bH1 (residues 19-29) in the head-group region on the matrix side of the IMM, transmembrane α-helix bH2 (residues 33-47) and the membrane region (residues 55-73) of bH3. In *B*, according to the assembly pathways in Fig. 7, subunits e and g associate with b to form the b-e-g intermediate. In *C*, subunit f is incorporated

subsequently to complete the protein components of the wedge; *D-H*, possible points of incorporation of lipids. In *E-G*, CDL3, LGH4 and LGH5 could be incorporated before or after the addition of e and g to b to form b-e-g, but before incorporation of f. In *H,* CD1 is incorporated after the formation of the b-e-g intermediate to complete the b-e-g-f complex.

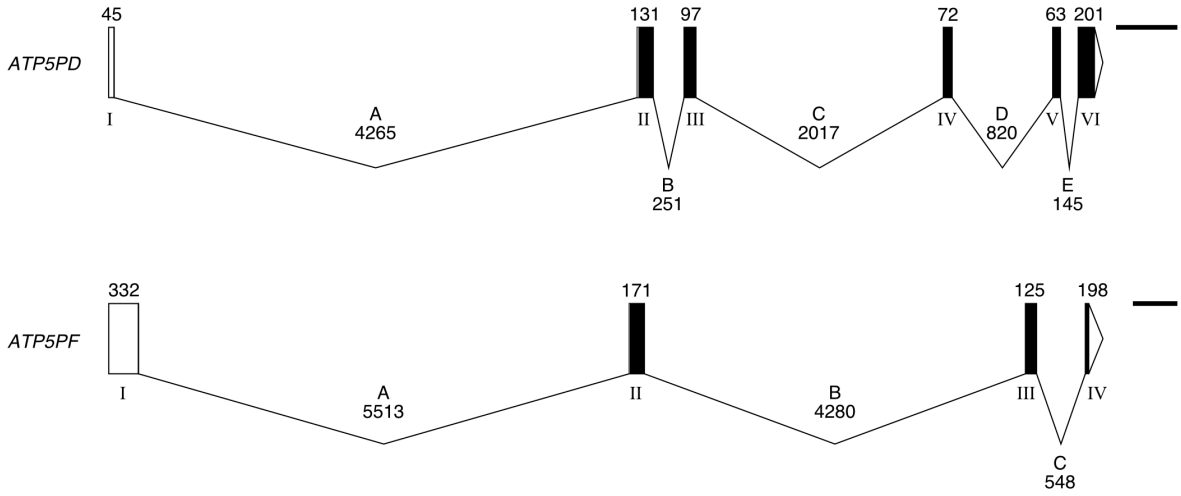

Fig. S2. Structures of the human genes *ATP5PD* and *ATP5PF* encoding subunits d and F_6, respectively, of ATP synthase. Exons are labelled with Roman numerals. Black and unfilled boxes in exons represent, respectively, protein coding and non-coding regions. Introns labelled with capital letters are depicted as intervening continuous lines. The sizes of introns and coding regions of exons are given in base pairs (bp). The scale bars on the right represent 500 bp. The exon-intron information was obtained from http://www.ensembl.org. The structures of *ATP5PD* and *ATP5PF* correspond to transcript ID reference ENST00000301587.9 and ENST00000400087.7. Images were drawn with the Exon-Intron graphic maker (http://wormweb.org/exonintron).

Table S1. Target sites for gRNAs employed in the disruption of human genes *ATP5PD* and *ATP5PF*, encoding subunits d and F_6 of human ATP synthase

gRNA	Sequence
ATP5PD-1	CTCTCAGAAACATACTGACC*
ATP5PD-2	TTTCAGGATCCCAAAATGGC
ATP5PF-1	GACGGCTGACCGAATGACAG*
ATP5PF-2	TCCTATACAGAAACTCTTTG

*Antisense sequence used for gRNA

Table S2. Primers employed in the amplification by PCR of regions targeted by gRNAs in *ATP5PD* and *ATP5PF*.

Primer	Sequence
ATP5PD-Forward	TCCCAACTGAAAATTCACCTCAT
ATP5PD-Reverse	AAGATCATCATGAAAATGCAAGGAT
ATP5PF-Forward	TTCCTGTTAGGAGCGGACAG
ATP5PF-Reverse	GAGATGAGCTCAGTGAAGGTCTAAT

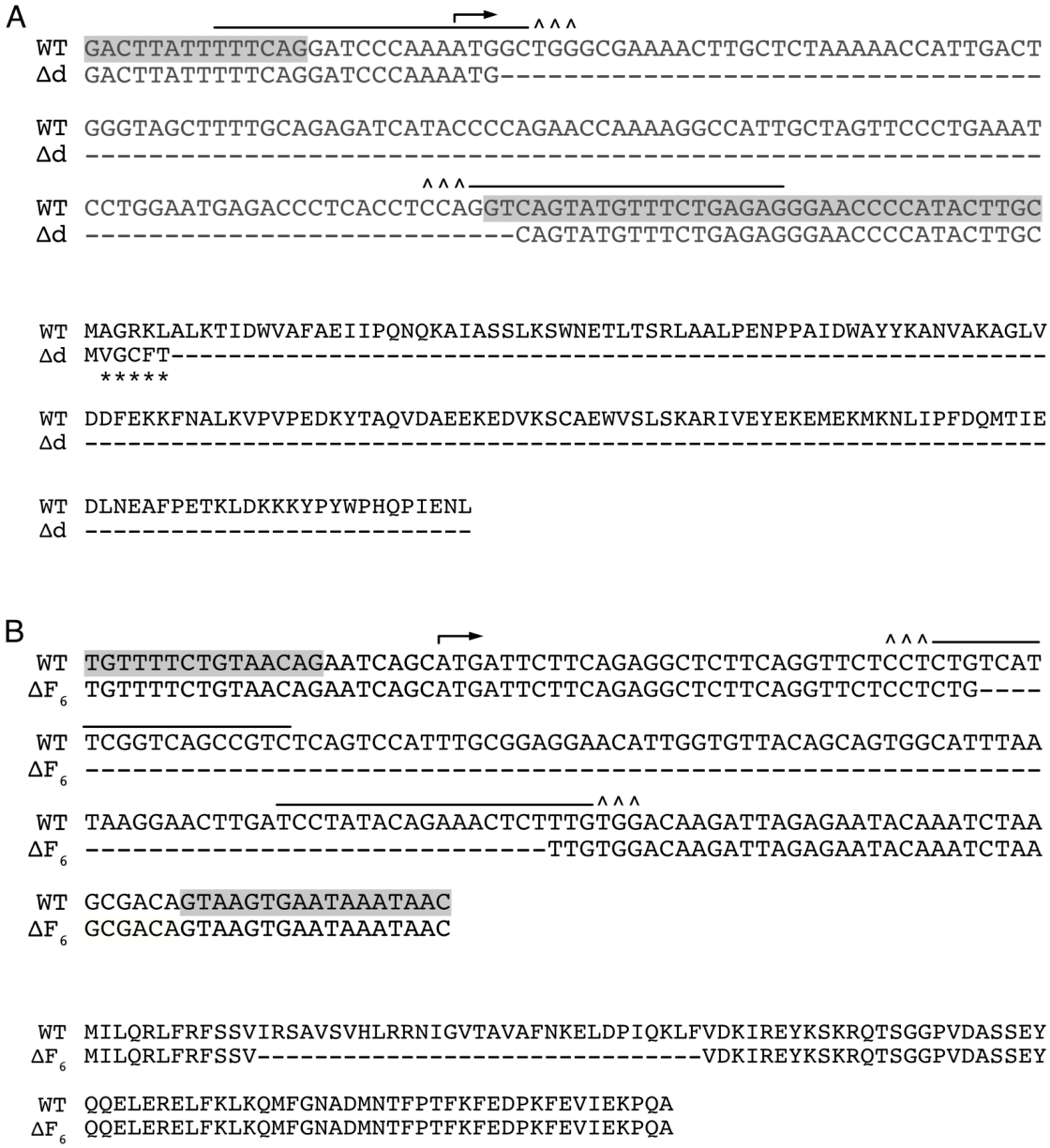

Fig. S3. Sequences of genes *ATP5PD* and *ATP5PF* disrupted by CRISPR-Cas9, and the encoded protein sequences in clonal HAP1-Δd and -ΔF_6 cells. The sequences are compared to the corresponding wild-type (WT) sequences. (*A*) *ATP5PD* and d subunit and (*B*) *ATP5PF* and F_6 subunit. Carets indicate the PAM (protospacer adjacent motif) sequences for each guide RNA, and solid lines for the target sequences for guide RNAs. The WT sequences are parts of intron A (grey box), all of exon II and part of intron B (grey box), aligned with the corresponding deleted sequences. The arrows indicate the start codons in exon II. The deleted

regions are denoted by dashed lines, and asterisks indicate non-matched amino acid to the wild-type.

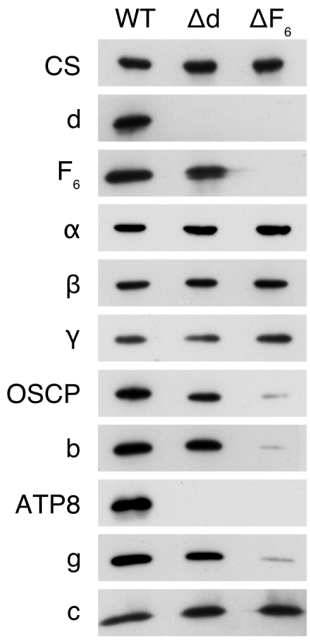

Fig. S4. Deletion of subunits d and F_6 from the peripheral stalk region of human ATP synthase in HAP1 cells. Mitoplasts from HAP1-WT, -Δd and -ΔF_6 clonal cells were extracted with *n*-dodecyl-β-D-maltoside. The extracts were fractionated by SDS-PAGE. Then the proteins were transferred to membranes and probed with antibodies against subunits indicated on the left. Citrate synthase (CS) was employed as a loading control.

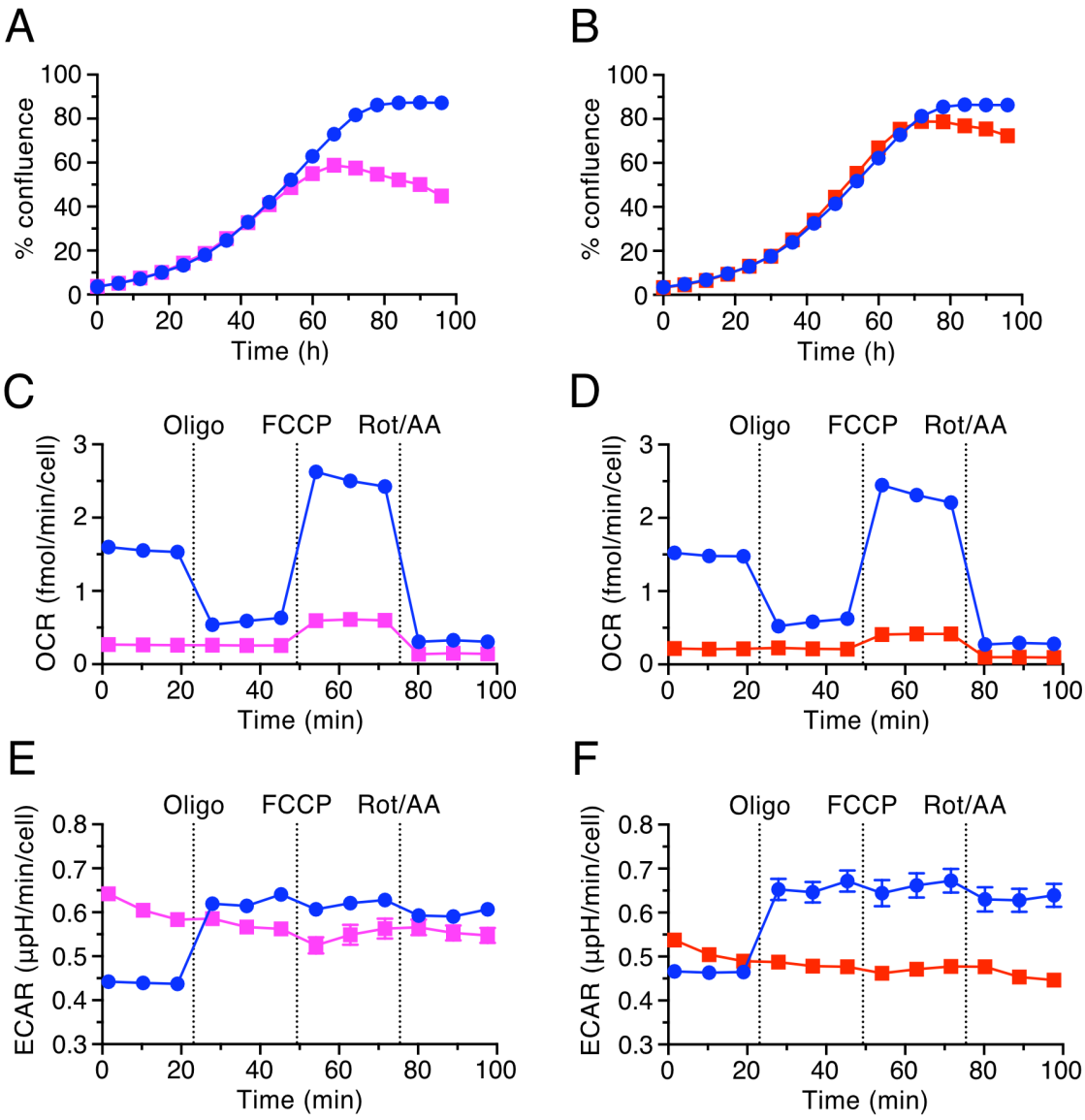

Fig. S5. Characteristics of HAP1-Δd cells and HAP1-ΔF$_6$ cells. (*A* and *B*), growth rates; (*C* and *D*) cellular oxygen consumption rates (OCR); (*E* and *F*) extracellular acidification rates (ECAR), of HAP1-WT cells (●) and HAP1 cells with disrupted genes for subunit d (■), or subunit F$_6$ (■). Growth rates were measured by seeding 10^5 cells into each well of a 6-well plate, and by monitoring their confluence over time. Initial confluences were adjusted to similar levels for comparison. The data points are the mean values ± SD (n = 3 wells). OCR and ECAR were measured with a Seahorse XF^{e}24 instrument, before and after sequential additions of oligomycin (Oligo), carbonyl cyanide-4-(trifluoromethoxy)phenylhydrazone (FCCP), and a mixture of rotenone and antimycin A (Rot/AA). Data represent the mean ± SEM (n=10 wells).

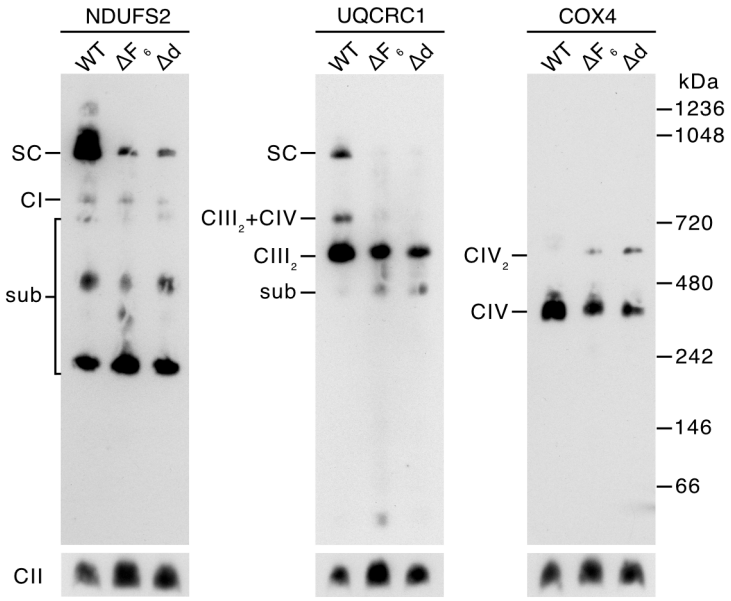

Fig. S6. Effect of deletion of subunits F_6 and d on the assembly of human electron transfer complexes. Mitochondrial membranes from HAP1-WT, -ΔF_6 and -Δd cells were extracted with digitonin (9 g/g protein), and the extracts were fractionated by BN-PAGE. Complexes were detected by western blotting with antibodies against complexes I (NDUFS2), III (UQCRC1) and IV (COX4). Complex II (CII-SDHA) provided a loading control. CI, complex I; $CIII_2$, complex III dimer; CIV, complex IV; CIV_2, complex IV dimer; $CIII_2$+CIV, complex III dimer plus complex IV; SC, supercomplex; sub, subcomplexes. The migration positions of standard proteins are shown on the right.

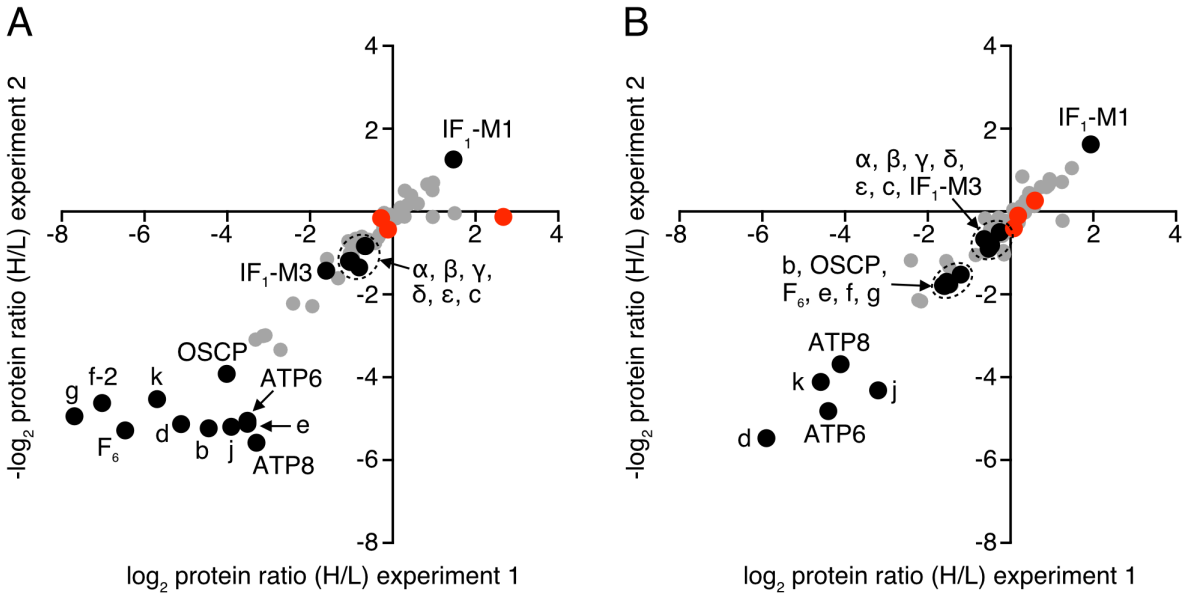

Fig. S7. Relative protein abundances in ATP synthase complexes purified from HAP1-ΔF$_6$ and HAP1-Δd cells. (*A*) and (*B*), respectively, immunocaptured ATP synthase from HAP1-ΔF$_6$ and HAP1-Δd cells. Samples were prepared from a 1:1 mixture of HAP1-WT cells with either HAP1-ΔF$_6$ cells or HAP1-Δd cells, that were differentially SILAC-labelled. The experiments were performed twice with reciprocal SILAC labelling orientations. The protein ratio is derived from a minimum of two peptide ratios from each experiment, except for ATP6 from HAP1-Δd in experiment 2, where the value is from a single peptide ratio. The ratios for proteins obtained in both experiments are plotted as a single point on a scatter plot as the log base 2 value. ●, ATP synthase subunits and forms of IF$_1$; ●, assembly factors ATPAF2, FMC1 and TMEM70; ●, all other proteins. In (*B*), the data point for Rab11 family-interacting protein 3, RAB11FIP3 (-5.40, 4.59) is outside the axes, in the upper left 'contaminant' quadrant. Protein ratios are given in *SI Appendix* Datasets S1-S4.

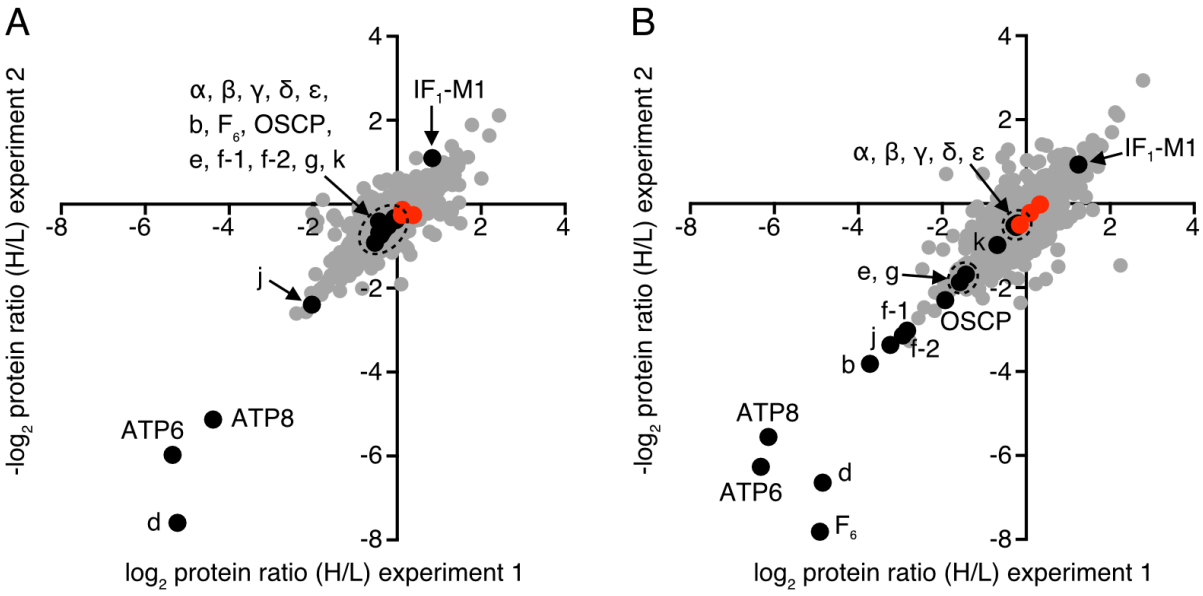

Fig. S8. Effects on protein relative abundance in mitoplast samples of HAP1 cells of the individual deletion of the d-subunit or F$_6$-subunit of human ATP synthase. Samples were prepared from a 1:1 mixture of HAP1-Δd or HAP1-ΔF$_6$ cells with HAP1-WT cells that were differentially SILAC-labelled. The experiments were performed twice, using reciprocal SILAC

labelling orientations. (*A* and *B*), the ratios for all proteins determined in both of the experimental labelling orientations are plotted as a single point on a scatter plot, as the log base 2 value, for mitoplast samples from HAP1-Δd and HAP1-ΔF_6 cells, respectively. The protein ratio is the median value derived from a minimum of two peptide ratios from each experiment, except for ATP synthase subunit ATP6 in the HAP1-Δd experiment 2, subunit f-2 in both HAP1-Δd experiments, and IF_1-M1 in the HAP1-Δd experiment 1, which only gave one peptide ratio. ●, ATP synthase subunits and the M1 mature forms of IF_1; ●, assembly factors ATPAF1, ATPAF2, and TMEM70; ●, all other identified proteins. Protein ratios are listed in Datasets S5-S8.

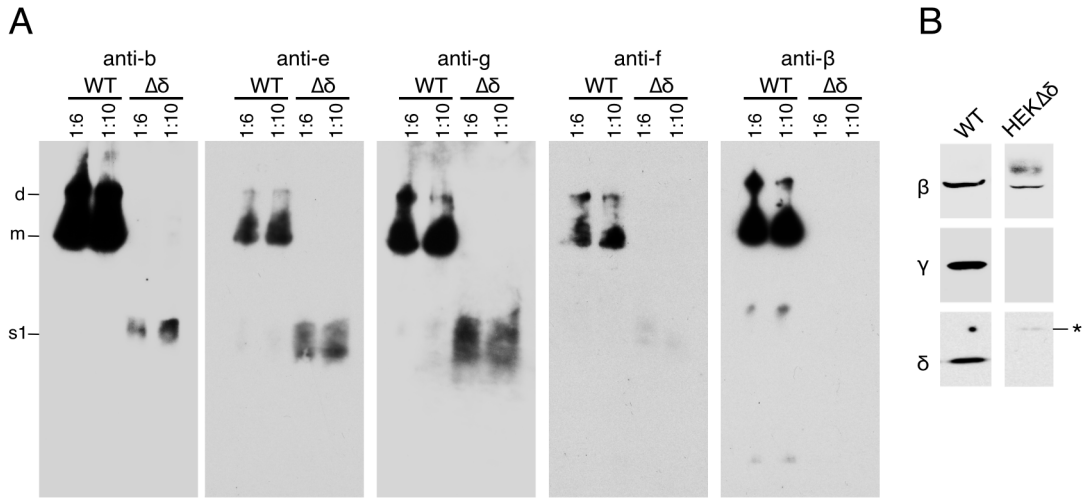

Fig. S9. Vestigial complexes of ATP synthase in HEK293-Δδ cells. (*A*) Fractionation of digitonin extracted complexes from mitoplasts of WT and HEK293-Δδ cells. Samples were extracted with digitonin (6 or 10 g/g protein) and the extracted complexes were fractionated by CN-PAGE, followed by Western blotting and probed with antibodies against subunits b, e, g, f and β (as indicated above the panels). The positions of complexes are shown on the left: d, ATP synthase dimer; m, ATP synthase monomer; s_1, subcomplexes containing subunits b, e, f and g. (*B*) SDS extracted proteins from wild-type (WT) and HEK293-Δδ cells were fractionated by SDS-PAGE and β-, γ- and δ-subunits were detected by western blotting. The

HEK293-Δδ cells have a weak band detected with an anti-δ antibody at *ca.* 17-18 kDa, marked with an asterisk.

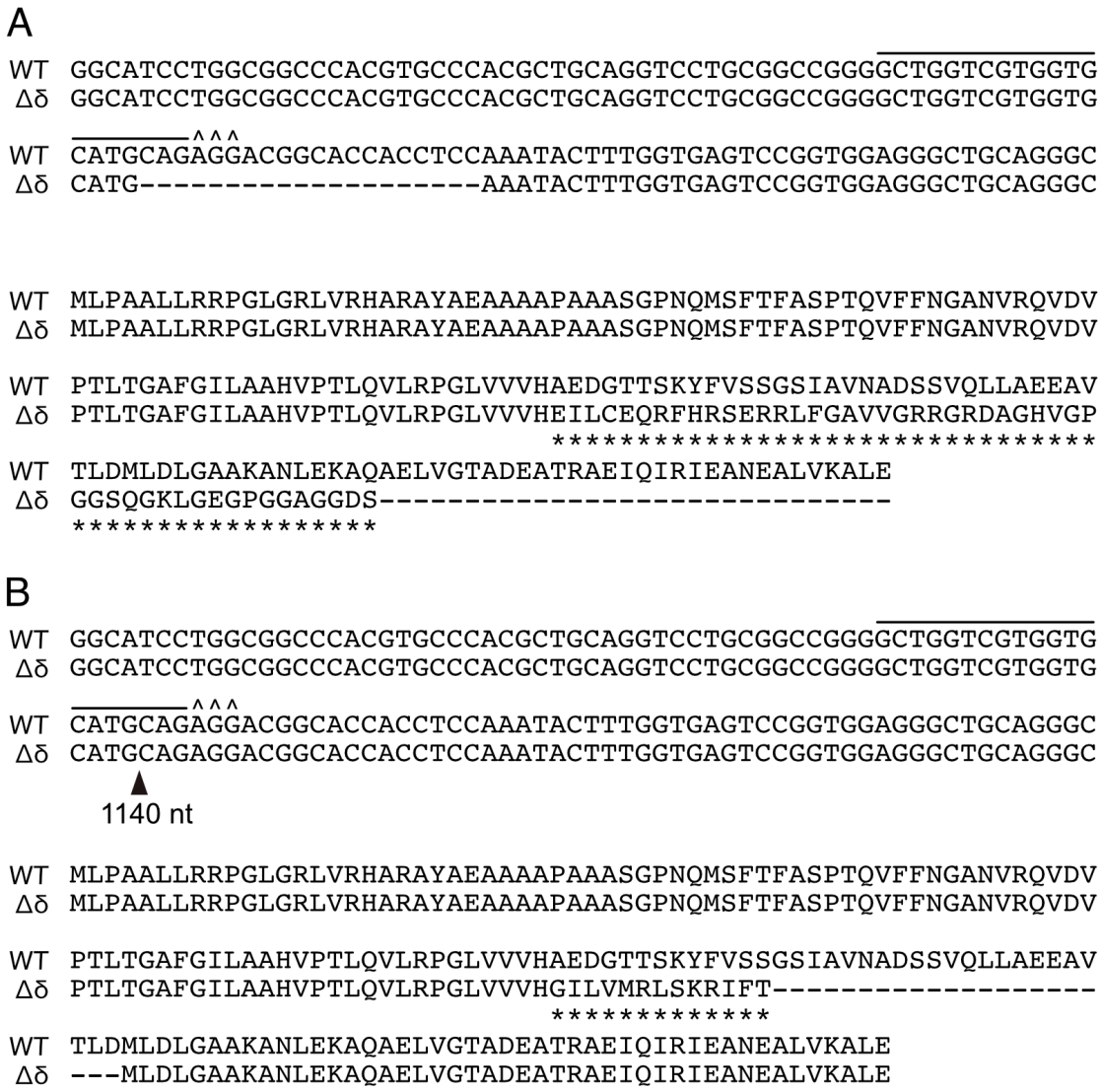

Fig. S10. Disruption of the gene for the δ-subunit of human ATP synthase in HEK293 Flp-In™ T-REx™ cells by CRISPR-Cas9. Clonal cells were derived with two differently edited versions of *ATP5F1D*, with in (*A*), a 20 bp deletion, and in (*B*), a 1140 bp insertion (sequence not shown) at the position indicated by the arrowhead. In the upper sections of (*A*) and (*B*), the disrupted DNA sequences are aligned with the wild-type (WT) sequence. The carets above the DNA sequences indicate the PAM (protospacer adjacent motif) sequence for the guide RNA, and solid lines the guide RNA target sequence. In the lower sections, the impact

of the deletions on the protein sequence of the δ-subunit are shown. Asterisks indicate changes in the protein sequence arising from the deletions, and the dashes indicate that the protein sequence has been terminated by the introduction of a stop codon. In (*A*) and (*B*), respectively, truncated versions of the δ-subunit were produced consisting of residues 1-88 followed by 50 and 13 unmatched residues. By internal initiation of the translation from four cryptic AUG codons, it is possible that the insertion might lead also to the production of residues 124-168 of the δ-subunit and three unrelated polypeptides (90, 62 and 117 amino acids long, not shown).

Table S3. Sources of Antibodies

Protein	Source	Antibody
ATP synthase δ	Proteintech	14893-1-AP
	ABclonal	A9929
ATP synthase b	Abcam	ab217062
ATP synthase c	Abcam	ab180149, ab181243
ATP synthase F_6	Abcam	ab224139
ATP synthase OSCP	Proteintech	66696-1-Ig
ATP synthase d	Proteintech	17589-1-AP
	In-house	Rabbit polyclonal against recombinant bovine protein
ATP synthase ATP8	Proteintech	26723-1-AP
PHB2	Proteintech	12295-1-AP
SDHB	Sigma	HPA002868
Strep II	Abcam	ab184224
TIM23	Abcam	ab230253